Extensive substrate recognition by the streptococcal antibody-degrading enzymes IdeS and EndoS

ABSTRACT

The cleavage of human IgG antibodies is a potent immune evasion mechanism utilised by some pathogenic bacteria. The *Streptococcus pyogenes* bacterium, which has the capacity to cause necrotising fasciitis, employs multiple enzymes to deactivate the human adaptive immune system. Two such proteins, IdeS and EndoS, prevent immune detection by ablating the immune effector functions of IgG, by cleavage and deglycosylation of its Fc region, respectively. Their fine specificity for IgG has led to a wide range of clinical and biotechnology applications, with IdeS having received clinical approval facilitating organ transplantation in hypersensitised individuals, while EndoS has found application in engineering antibody glycosylation. Here, we present crystal structures of IdeS and EndoS in complex with their IgG1 Fc substrate, with both enzymes exhibiting exquisite target specificity. The IdeS protease is shown encasing the antibody hinge target, but also recognises the Fc globular domains. In contrast, the glycan hydrolase domain in EndoS traps the Fc glycan in a flipped-out conformation, while additional antibody specificity is driven by protein recognition by the so-called carbohydrate binding module. Understanding the molecular basis of antibody recognition by bacterial enzymes will facilitate the development of next-generation enzymes.

INTRODUCTION

The bacterium *Streptococcus pyogenes* secretes enzymes evolved to specifically deactivate the adaptive immune system (1). Infection with *S. pyogenes* can be mild, causing for example throat infections, but at the other extreme can cause terminal necrotising fasciitis (2). Two of *S. pyogenes'* immune evasion factors are the immunoglobulin-degrading enzyme of *S. pyogenes* (IdeS) (3) and endoglycosidase S (EndoS) (4), both of which directly target and cleave IgG antibodies (Fig. 1), and thereby impede immune recruitment mediated by the antibody Fc domain. The specificity of these enzymes for IgG antibodies (3, 4) has led to the development of a wide range of clinical and biotechnology applications and this has warranted extensive studies of their enzymology.

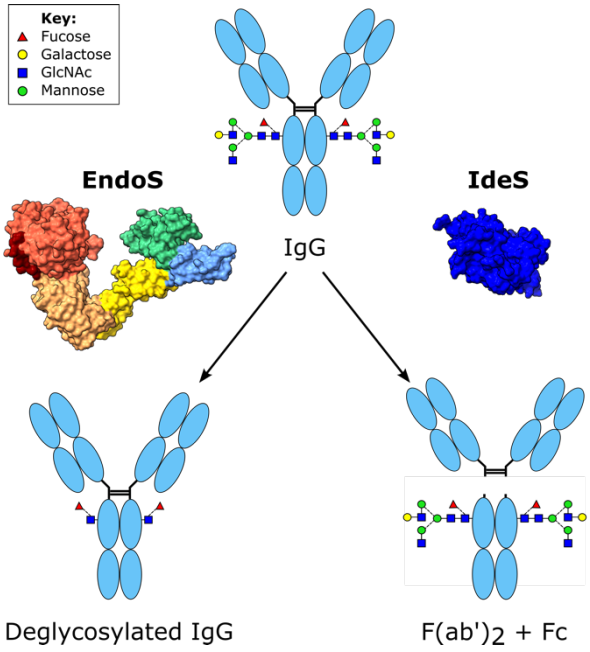

Figure 1: Schematic diagram of IgG cleavage by IdeS and EndoS. Cleavage of biantennary, complex-type N-linked glycans at N297 in the IgG Fc region by EndoS leaves a single (a)fucosylated GlcNAc monosaccharide on each heavy chain, while cleavage of IgG by IdeS yields $F(ab')_2$ and Fc fragments. IgG is depicted in light blue; glycans are depicted using the SNFG nomenclature (5).

Of the two immune evasion factors, IdeS is most advanced in clinical development. The enzyme targets IgG by cleaving within the lower hinge region, yielding $F(ab')_2$ and Fc fragments (3, 6, 7), an activity which has enabled its development, under the name Imlifidase, as a pre-treatment for kidney transplantation in hypersensitized patients with chronic kidney disease (8-16). Along with EndoS, it has further potential use in the deactivation of pathogenic antibodies in

autoimmune disorders (11, 17-26), deactivation of neutralising antibodies for *in vivo* gene therapy (27), and for the potentiation of therapeutic antibodies by deactivating competing serum IgG (28, 29). Imlifidase has also been used in combination with EndoS for inactivation of donor-specific antibodies in murine allogeneic bone marrow transplantation (10).

The endoglycosidase EndoS has additional biotechnological applications in engineering antibody glycosylation (30): it hydrolyses the β-1,4 linkage between the first two N-acetylglucosamine (GlcNAc) residues within biantennary complex-type N-linked glycans on IgG Fc (4) (Fig. 1). A related enzyme from serotype M49 of *S. pyogenes*, EndoS2 (31), also targets IgG, but exhibits a broader glycan specificity (32). Moreover, mutants of both enzymes have been utilised in transglycosylation of various glycoforms to intact IgG (33, 34), all of which collectively enable precise antibody glycan remodelling.

It is still unclear, however, how exactly these enzymes specifically target and degrade IgG. Full cleavage of an antibody by IdeS occurs in two distinct steps, in which the second chain is cleaved more slowly (6, 7); this observation, along with the finding that IdeS exhibits low activity towards synthetic hinge peptides (35), suggests a more extensive recognition interface with the target IgG. Similarly, multiple domains within EndoS contribute to substrate recognition and catalysis (36-38).

Here, we sought to understand the molecular basis behind the unique substrate specificity of these enzymes using X-ray crystallography. To promote crystallization of the protein complexes, we mutated IgG Fc residue E382, which consistently forms salt bridge interactions in typically-observed Fc crystal lattice interactions, in order to discourage Fc self-crystallization. We present crystal structures of IdeS and EndoS in complex with their IgG1 Fc substrates, to a resolution of 2.34 Å and 3.2 Å, respectively, which will facilitate their continued clinical and biotechnological development.

RESULTS AND DISCUSSION

Crystallization of protein complexes using IgG1 Fx

The co-crystallization of Fc with enzymes is notoriously difficult. In order to overcome the problem of selective crystallization of the highly crystallizable Fc domain we sort to eliminate this property from the Fc. We have observed, from looking at structures currently in the PDB, that IgG Fc usually crystallises in the $P2_12_12_1$ space group. We studied the unit cell composition and crystal lattice contacts of a typical Fc structure (PDB code 3AVE) in order to identify residues that are important in this favourable packing arrangement. As calculated with the “crystal contacts” function in ChimeraX (39), using a set distance maximum of 3 Å, model 3AVE forms contacts with eighteen residues, in eight symmetry-related molecules. We identified residue E382, which forms a salt bridge with R255 of a symmetry-related molecule in both of its Fc chains, and thus comprises four of these contacts (Fig. 2A). We hypothesised that mutation of E382 in IgG Fc would hinder its self-crystallization, and therefore designed three IgG1 Fc mutants: Fc E382R, Fc E382S and Fc E382A, which collectively we have termed as “Fx” mutants.

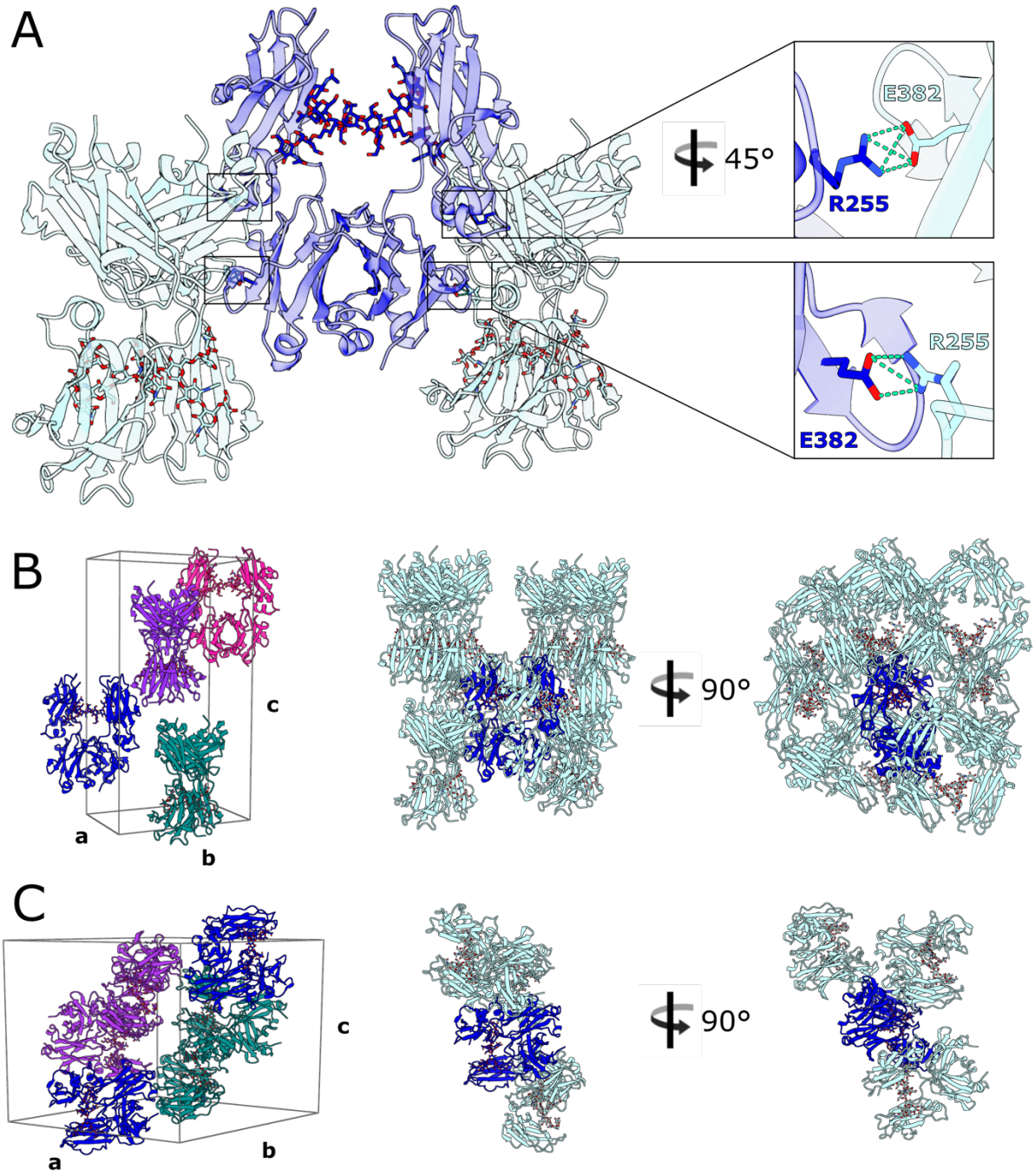

Figure 2: IgG1 Fc crystal lattice contacts. (A) Salt bridge interactions present between E382 and R255 in wild-type IgG1 Fc crystal lattice (PDB code 3AVE). Origin Fc is depicted in dark blue; symmetry-related Fcs are depicted in light blue. N297 glycans and E382/R255 residues are shown as sticks and coloured by heteroatom; hydrogen bonds are depicted as green dashes. Models are shown with 50 % transparency to highlight E382-R255 contacts. (B) Crystallization of wild-type IgG1 Fc (PDB code 3AVE) in $P2_12_12_1$ space group, with orthorhombic unit cell a=49.419 Å, b=78.471 Å, c=143.758 Å, $\alpha=\beta=\gamma=90°$. (C) Crystallization of IgG1 Fc containing E382S mutations in atypical space group $P3_221$, with altered unit cell dimensions $a=b$=106.78 Å, c=104.01 Å, $\alpha=\beta=90°$,$\gamma=120°$. (B/C) Origin molecules are depicted in dark blue, symmetry-related molecules in unit cells are depicted in purple, teal and pink, showing transformation axes in the x, y and z dimensions, respectively. Symmetry-related Fcs that contact the origin Fc, as calculated in ChimeraX (39) are shown and depicted as in (A).

We obtained crystals of the Fc E382S mutant, which were found to have grown in an atypical space group $P3_221$ (Table S1), with altered unit cell dimensions (Fig. 2C). The structure was solved by

molecular replacement (using 3AVE as a search model) and refined to a resolution of 3.04 Å. Analysis of the crystal contacts revealed that the mutant Fc makes fewer interactions with symmetry-related molecules (twelve interactions between the "origin" Fc and three symmetry-related Fcs) in its altered unit cell (Fig. 2B,C). This indicates that mutation of residue E382 has hindered self-crystallization of the Fc by weakening its crystal packing interactions.

Crystallization of IdeS-IgG1 Fc complex

Using our panel of IgG1 "Fx" mutants, IdeS from *Streptococcus pyogenes* (strain MGAS15252), containing a C94A mutation to abolish catalytic activity, was crystallised in complex with IgG1 Fc (E382A mutant), in space group *C*121 (Table S2). Electron density is present for residues 43-339 in IdeS and residues 228-445 and 229-444 for chains A and B in IgG1 Fc, respectively. We additionally observe clear density for eight monosaccharide residues at the N-linked glycosylation site (N297) for chain B, comprising a fucosylated biantennary glycan with terminal β1,2-linked GlcNAcs, and seven monosaccharide residues for that on chain A, comprising a fucosylated biantennary glycan with a single β1,2-linked GlcNAc on the mannose 6-arm. The final structure was refined to 2.34 Å and is depicted in Figure 3.

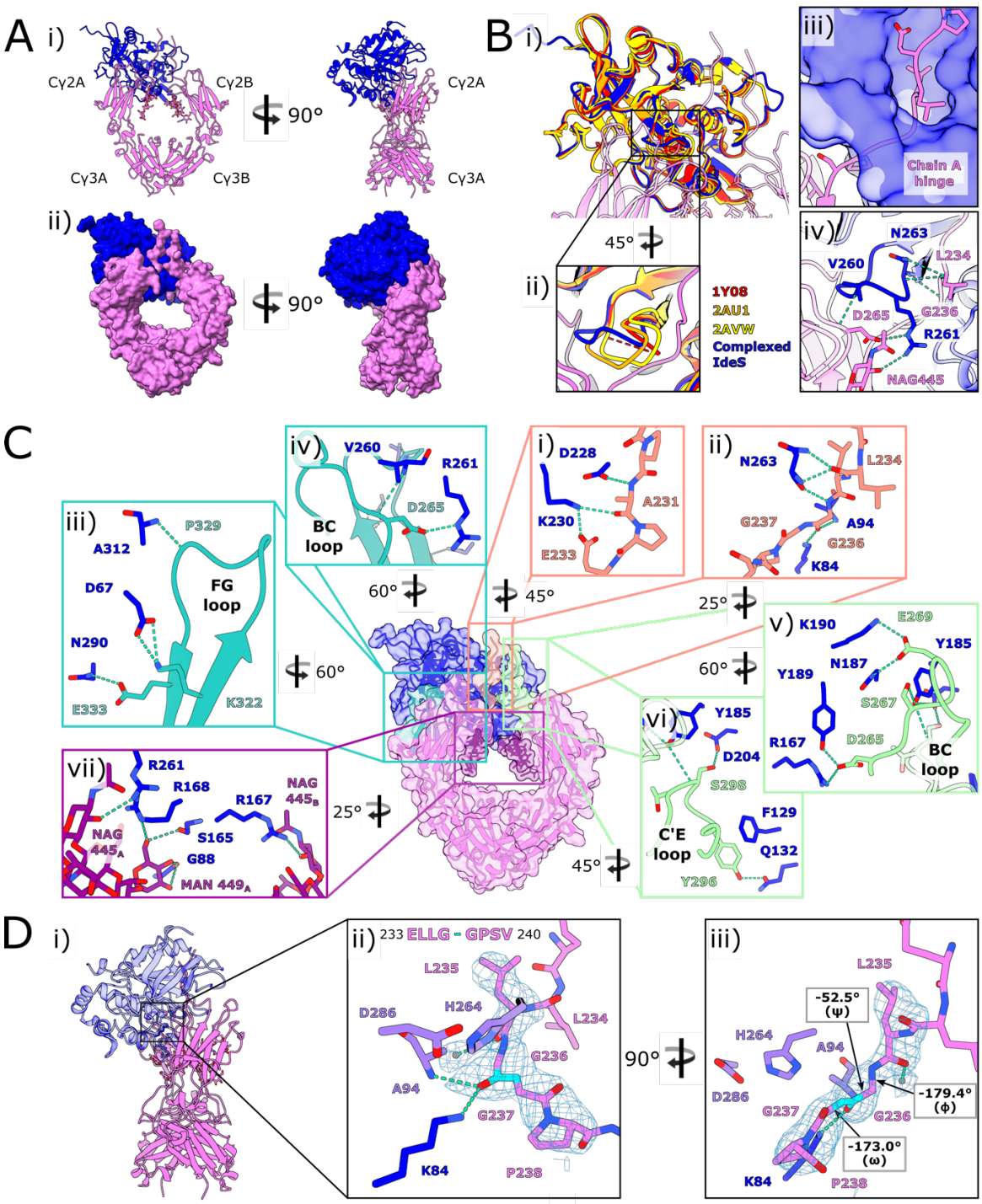

Figure 3: Crystal structure of IdeS in complex with IgG1 Fc. (A) Overall structure of the complex, depicted as a cartoon (i) with N-linked glycans as sticks, and as a surface (ii). (B/i) Superposition of complexed IdeS with deposited apo structures. (ii) Focused view of prosegment binding loop. (iii) Surface representation of prosegment binding loop, with Fc hinge depicted in cartoon/stick form. (iv) Interaction of prosegment binding loop of IdeS with IgG1 Fc. (C) Binding interface of IdeS with regions of IgG1 Fc: chain A upper (i) and lower (ii) hinge, chain A FG (iii) and BC (iv) loops, chain B BC (v) and C'E loops (vi), and N-linked glycans (vii). (D/i) Side view of complex shown with 50 % transparency with positions of catalytic residues A94, H264, D286 and K84 highlighted. (ii/iii) Focused view of active site with chain A hinge peptide bound. An omit map weighted at 3.0σ is shown around residues 235-238 of the Fc and a catalytic water (depicted as a grey circle). (iii) Phi (φ), psi (ψ) and omega (ω) peptide torsion angles for the scissile peptide bond are indicated. (A/B/C/D) IdeS is depicted in blue; IgG1 Fc is depicted in pink. Regions depicted as sticks are coloured by heteroatom, with oxygen atoms in red and nitrogen atoms in blue. Hydrogen bonds are depicted as green dashes.

Overall structure

The crystal structure shows asymmetric binding of an IdeS monomer across the Cγ2 domains of the Fc (Fig. 3A). Although a molecule's crystalline state doesn't necessarily represent its biologically-relevant form, the combination of evidence from crystallography (Fig. 3A), analytical size exclusion chromatography (Fig. S1) and kinetic analyses by Vindebro *et al*. (40) allows us to conclude that IdeS functions predominantly in a monomeric form. The enzyme appears to clamp down over the lower hinge region of one Fc chain, creating a cavity in which the catalytic residues are brought into close proximity with the cleavage site. Consequently, the Cγ2 domain in chain A is pulled away from chain B, reflected in a greater root mean squared deviation between Cαs in the Cγ2 domains (1.347 Å compared to 0.675 Å in wild-type Fc 3AVE, calculated in ChimeraX (39) for residues 237-341) and higher atomic B factors in this domain (Fig. S2A).

IdeS comprises an α/β fold, with ten alpha helices and ten beta strands as calculated by ChimeraX (39) (Fig. S2B). Complexed IdeS (Mac-2 isoform) shows some sequence diversity between residues 111-205 compared to the three published apo IdeS/Mac-1 structures (41), but a structural alignment shows very few deviations (Fig. 3B/i, Fig. S2C). We note that the loop located between beta strands five and six, equivalent to the "prosegment binding loop" in other papain superfamily cysteine proteases (42-44), is modelled in distinct conformations for each of the apo structures and is not included within 1Y08 (45) (Fig. 3B/ii), signifying its inherent flexibility in the apo form. In complexed IdeS, the loop curls upwards to accommodate the Fc hinge within the active site cavity and makes contacts with protein and carbohydrate residues (Fig. 3B/ii,iii,iv). Notably, the protein sequence within this loop is conserved between Mac-1 and Mac-2, and contains H264 (H262 in Mac-1) from the catalytic triad.

Alanine mutations to N257, R259 and V263 (as numbered in Mac-1) within this loop were found to have little effect on IdeS-IgG binding and catalytic activity (46). Our structure shows, however, that only R259 (R261 in Mac-2) interacts with the Fc *via* its side chain (Fig. 3B/iv), and that a large proportion of the interactions involve the IdeS backbone, whose conformation won't be significantly altered by alanine mutations. The inability of IdeS to cleave IgG hinge-mimicking peptides (35) also indicates an occlusion of the active site in the absence of substrate, especially given the strong potential of hydrogen bonding and hydrophobic interactions observed at the Fc hinge (discussed in the following section). We therefore conclude that this loop is important for IdeS function, specifically in mediating substrate access to the active site.

Extended exosite binding

It has long been suspected that IdeS must recognise its sole substrate IgG with exosite binding (35, 45, 46). Our structure now reveals that IdeS binds across both chains of the Fc and its carbohydrate groups. Unsurprisingly, the most extensive interface is formed with the Fc chain being cleaved (chain A in our structure) (Fig. 3C/i-iv), with an interface area of 1392 $Å^2$ and a solvation free energy gain upon interface formation of -15.9 kcal/mol, as calculated by PISA (47). The interface extends across the entire hinge region (P228-S239), with hydrogen bonds formed with A231, E233, L234, G236 and G237 (Fig. 3C/i,ii) and significant hydrophobic forces predicted by PISA. Within the Cγ2 domain, IdeS interacts with residues in proximity of the Fc BC loop (important for stabilising an "open" conformation of the prosegment binding loop, as discussed above) and the FG loop (Fig. 3C/iii,iv).

A secondary interface is formed across chain B of the Fc, with an interface area of 802.3 $Å^2$ and a solvation free energy gain of -7.7 kcal/mol. A smaller proportion of the Fc hinge contributes (A231-G237), but PISA predicts favourable hydrophobic interactions here, albeit not to the same extent as chain A. The majority of hydrogen bonds within this interface occur between BC loop residues (V264-E269) (Fig. 3C/v). In contrast to chain A, the C'E loop, which contains the N-linked glycan at N297, also

forms part of the interface in chain B (Fig. 3C/vi). IdeS additionally interacts with both N297 glycans (Fig. 3C/vii); the lack of electron density for any monosaccharides past β1,2-linked GlcNAc suggests that any further glycan processing wouldn't affect complex formation, and that IdeS can accommodate IgG with heterogenous glycosylation.

Although IdeS interacts with both chains in the Fc hinge simultaneously, following cleavage of the first chain, the complex would need to dissociate before the second cleavage could occur. This observation is also evidenced by detection of single-cleaved Fc in enzymatic assays and in clinical studies (6, 8, 40, 48). We suspect that the binding interface is altered for single-cleaved Fc and that this explains its slower rate of cleavage (6, 7, 40). PISA predicts that both Fc chains are important in complex formation, so the interface with both chains simultaneously likely reflects how IdeS has evolved to recognise IgG as its sole substrate. It is interesting to note that, aside from the hinge region, IdeS binds Fc regions also implicit in FcγR binding, an observation also inferred by its ability to counteract Fc-mediated effector functions by competitive binding inhibition (41). Moreover, we observe that IdeS residues interacting with the Fc are largely conserved between Mac-1 and Mac-2, and any substitutions are mostly to similar amino acids, which provides a structural rationale for the near identical catalytic activity measured for these two isoforms (49).

Active site interface

Analyses of the published IdeS apo structures have previously revealed insights into its catalytic mechanism (45, 46). A structural overlay of complexed and apo IdeS reveals little to no variation in placement of catalytic triad residues C94, H264 (H262 in Mac-1) and D286 (D284 in Mac-1) (Fig. S2D), indicating that the enzyme activity is only limited by the position of the flexible active site loop and substrate availability. We observe clear density for the Fc chain A hinge region bound within the active site cavity (Fig. 3D/ii,iii): the carbonyl oxygen of G236 is hydrogen bonded to the amide nitrogen of the catalytic cysteine (mutated to alanine here) and the side chain of K84, which collectively form the oxyanion hole, as predicted (45, 46). Binding of the hinge clearly distorts the peptide backbone at G236 in order to promote scissile bond cleavage (Fig. 3D/iii); this residue is thus identified in Molprobity (50, 51) as a Ramachandran outlier.

The catalytic cysteine rotamer within complexed IdeS very likely matches that seen in the wild-type IdeS crystal structure (serotype M1; PDB code 2AU1; Fig. S2D/ii). In this position, its sulphur is in a plane with both the basic nitrogen within the H264 side chain and the alpha carbon within the scissile peptide bond, likely facilitating thiol deprotonation by H264 and subsequent nucleophilic attack on the peptide substrate. We observe a water molecule within the active site, maintained in position *via* hydrogen bonds to L92, G95 and V171 backbone atoms (within IdeS), and the carbonyl oxygen of L235 in the Fc hinge (Fig. 3D/ii,iii); this is likely employed as a nucleophile to catalyse hydrolysis of the thioester bond within a tetrahedral intermediate linking the G236 carbonyl to the catalytic cysteine, in order to liberate the carboxylic acid moiety on G236 and regenerate the thiol group. Some details of the catalytic mechanism of IdeS remain to be experimentally investigated and are beyond the scope of this present work; for example, whether thiol deprotonation occurs before or after substrate binding, and which reaction step is rate-limiting. Such questions have been debated in the literature for cysteine proteases in general (52-57) and will need to be investigated further.

Crystallization of EndoS-IgG1 Fc complex

Structures for several endoglycosidases, in apo forms and in complex with their glycan substrates (32, 36, 38, 58-65), have been solved. Here, we present the structure of truncated EndoS (residues 98-995, as described previously (36)) in complex with its IgG1 substrate (Fc E382R mutant). An inactive version of EndoS was generated by the inclusion of D233A/E235L mutations as described previously (38). The

complex crystallised in space group $P2_12_12_1$ and was refined to a resolution of 3.2 Å (Table S3); the final structure is depicted in Figure 4.

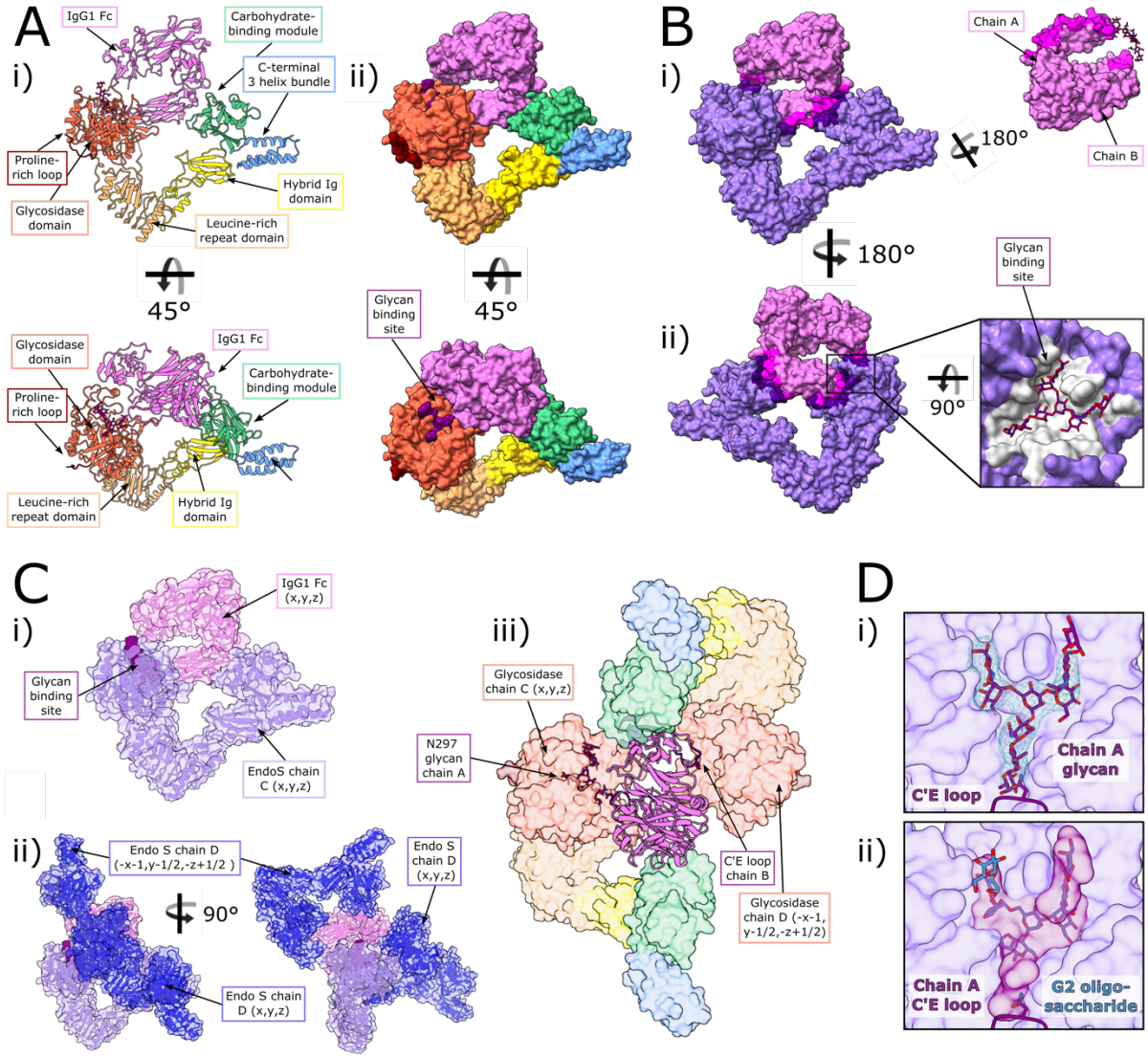

Figure 4: Crystal structure of EndoS in complex with IgG1 Fc. (A) Overall structure of complex, depicted in cartoon (i) and surface (ii) form. EndoS regions are coloured as follows: proline-rich loop, maroon; glycosidase domain, red; leucine-rich repeat domain, orange; hybrid Ig domain, yellow; carbohydrate-binding module, green; C-terminal 3 helix bundle, light blue. IgG1 Fc is depicted in pink and its N-linked glycan is depicted in purple. (B) EndoS-Fc binding interface. IgG1 Fc is depicted in pink; EndoS is depicted in lilac. Interfacing residues in IgG1 Fc and EndoS (identified by PISA (47)) are coloured magenta and indigo, respectively. (i) Front view of complex and view of Fc alone after 180° rotation in x and y directions. (ii) Back view of complex and focussed view of glycan binding site (interfacing residues are coloured silver). (C) EndoS-Fc crystal packing and stoichiometry. (i) Front view of complex; (ii) front and side view of complex, showing second molecule of EndoS (chain M) in unit cell and its symmetry-related copy at (-x-1,y-1/2,-z+1/2) which also binds the Fc homodimer. (iii) Bottom-up view of complex, coloured as in (A), depicting 1:1 stoichiometry of EndoS binding each glycan in IgG1 Fc. (D) Binding site of IgG1 Fc glycan. (i) Overlay of G2 substrate (from PDB deposition 6EN3) with EndoS-Fc complex, with the modelled glycan depicted as a surface. (ii) Omit map around N-linked glycan in the EndoS-Fc complex, weighted at at 4.0σ.

Overall structure

Our structure of EndoS shows the same "V" shape as observed in its previously solved structures (36, 38), comprising, from the N- to the C terminus: a proline-rich loop (residues 98-112) a glycosidase

domain (residues 113-445), a leucine-rich repeat domain (residues 446-631), a hybrid Ig domain (residues 632-764), a carbohydrate-binding module (CBM; residues 765-923) and a C-terminal three-helix bundle domain (C-3HB; residues 924-995) (Fig. 4A/i). One Cγ2 domain in IgG Fc (chain A in our structure) binds across the termini of the "V", between the glycosidase domain and CBM, with the rest of the antibody remaining exposed to the surrounding solvent. The N-linked glycan on this chain is flipped out from its usually-observed position between the two Cγ2 domains (66) and is bound within the glycosidase domain cavity (Fig. 4A). A structural overlay with full length EndoS in complex with its G2 oligosaccharide substrate (PDB code 6EN3) shows that the overall morphology and domain organisation of EndoS is approximately maintained (Fig. S3A/i,ii), apart from a slight shift of the C-3HB, likely due to a pinching of the CBM around the Fc as it binds.

Binding Interface

Our structure of the EndoS-Fc complex reveals how one Cγ2 domain of the Fc binds across the glycosidase domain and CBM (Fig. 4B), corroborating previous findings that these two regions are important for IgG Fc binding (36) and glycan hydrolysis (37), and the identification of the Fc Cγ2 homodimer as an EndoS substrate (37). As calculated by PISA (47), the interface between chain A of the Fc and EndoS (chain C) comprises an area of 1350.6 $Å^2$ and yields a solvation free energy gain of -9.2 kcal/mol. A small number of contacts are also predicted between EndoS and the second Cγ2 in the Fc (chain B; Fig. 4B); although these are unlikely to be necessary for complex formation given that EndoS can cleave the Fc Cγ2 lacking the hinge region (likely monomeric) (37).

Interestingly, although previous work has indicated that it can bind galactose (albeit with low affinity) (37), the CBM doesn't bind carbohydrate, and the N- and C-terminal 3 helix bundles, which are homologous to IgG-binding protein A from *Staphylococcus aureus* (38, 67), don't bind protein. A structural overlay of complexed EndoS with full-length EndoS (PDB code 6EN3) shows no contacts between the N-3HB and the Fc (Fig. S3A), thus its contribution to EndoS-IgG binding and glycan hydrolysis is likely solely due to stabilisation of the glycosidase domain, as suggested previously (38). Indeed, existence of the crystal structure is evidence in itself that EndoS forms a stable complex with IgG in its absence.

Serotype M49 of *S. pyogenes* expresses EndoS2 (31), another IgG-specific endoglycosidase with a similar domain structure to EndoS, but with a broader glycan specificity (32). Hydrogen-deuterium exchange mass spectrometry of the EndoS2-IgG1 complex revealed large changes in deuterium uptake for the glycosidase and CBM regions, but very few changes were observed within the antibody surface (32), indicating that its binding interface is small. This result supports the idea that the protein-protein interface is not particularly extensive. In contrast, mutation of residues within the glycan binding site of EndoS and EndoS2 completely diminished their hydrolytic activity (32, 38). It is therefore apparent that glycan recognition is the most important aspect of EndoS activity, with other domains such as the CBM acting to enhance the catalytic efficacy (36, 37).

Binding mechanism

Within the crystal, we observe a 2:1 stoichiometry of EndoS to the IgG Fc homodimer in the complex (Fig. 4C). The N297 glycan within chain A of the Fc binds the first EndoS molecule (chain C) in the asymmetric unit; its counterpart in chain B, although not fully visible in the electron density, is clearly binding a symmetry-related copy of the second EndoS molecule (chain D) present in the asymmetric unit (Fig. 4C). Previous work has indicated that EndoS is largely monomeric in solution (36, 38), and it appears that the recognition of IgG Fc glycans whilst in a "flipped out" state allows space for two enzymes to bind simultaneously. Although EndoS crystallised here is lacking the N-3HB domain, a structural superposition with full-length EndoS (Fig. S3A) suggests 2:1 binding would be able to occur in its presence.

We observe clear electron density for the chain A N297 glycan within the EndoS carbohydrate-binding cavity previously identified (Fig. 4D/i,ii) (38). It appears that both Fc glycans have been captured in a high energy conformation, given the identification of outliers by MolProbity (50, 51) in the chain A C'E loop, and the incomplete electron density of its chain B counterpart. It is fascinating to observe the glycan trapped in this "open" state, and this substantiates several recent studies documenting the existence of IgG Fc glycan conformational heterogeneity (68-72). Superposition of complexed IgG with a wild-type Fc (PDB code 3AVE) illustrates that this open state is governed by movement of the C'E loop only (Fig. S3B), although it is possible that the lower resolution of the data is masking small chain shifts.

Perspectives

The crystal structures presented here provide a structural rationale for the unique properties of these two enzymes, and can now be exploited for optimisation of their long-term clinical and biotechnological applications. Not only will they enable the design of antibodies resistant to cleavage by these enzymes, whose potency can be strengthened with removal of serum IgG (28, 29), they will also be invaluable in the synthesis of immunologically-distinct enzyme variants which retain identical activity, for their repeated therapeutic use. EndoS mutants have already been designed to expand its ability to engineer antibody glycosylation (33, 34); structural information presented here will allow this to be extended further.

METHODS

Protein Expression and Purification

IdeS/EndoS

IdeS containing a C94A mutation (residues 41-339, gene accession number AFC66043.1) and EndoS containing D233A/E235L mutations (residues 98-995, as described previously (36, 38)) were synthesised by NBS Biologicals and cloned into pET21a(+) vectors. Constructs were expressed in *E.coli* BL21 (DE3) cells. Cells were grown at 37 °C in Terrific Broth (Melford) in the presence of 100 mg/mL ampicillin and 34 mg/mL chloramphenicol, until an OD_{600} of 0.8 was reached, following which protein expression was induced with addition of 1 mM IPTG and cells were left to shake overnight at 25 °C. Cells were extracted by centrifugation at 6,220 x *g* for 20 minutes, resuspended in lysis buffer (PBS containing DNAse1 and lysozyme), homogenised using a glass homogeniser and broken apart using a cell disruptor. The remaining sample was centrifuged first at 3,100 x *g* for 20 minutes, then again at 100,000 x *g* for one hour, to remove any remaining cell debris and cell membranes. The resulting supernatant was subsequently filtered through a 0.2 μm pore. Proteins were purified from the supernatant using affinity chromatography with a HisTrap HP column (Cytiva) followed by size exclusion chromatography with a Superdex 75 16/600 column (Cytiva), in 10 mM HEPES, 150 mM NaCl, pH 8.0.

IgG1 Fcs

Residues 221-444 from IgG1 Fc containing E382R/S/A mutations were synthesised by NBS Biologicals and cloned into a pFUSE-hIgG1-Fc vector. Fcs were transiently expressed in FreeStyle293F cells (Thermo Fisher) and harvested after seven days by centrifugation at 3,100 x *g* for 30 minutes. Supernatant was filtered through a 0.2 μm pore and antibodies purified by affinity purification with a HiTrap Protein A HP column (Cytiva), followed by size exclusion chromatography with a Superdex 200 16/600 column (Cytiva) in 10 mM HEPES, 150 mM NaCl (pH 8.0).

Protein Complex Formation

IdeS/EndoS were combined with IgG1 Fcs in a 1:1 molar ratio and applied to a Superdex 200 16/600 column (Cytiva) equilibrated in 10 mM HEPES, 150 mM NaCl (pH 8.0). Fractions corresponding to the main peak were pooled for crystallization.

Protein Crystallization

Purified proteins were exchanged into 50 mM HEPES, 150 mM KCl (pH 7.5) prior to crystallization. Crystal trays were set up using an Oryx4 robot (Douglas Instruments), and all crystals were grown by sitting drop vapour diffusion. Crystals of the IdeS-Fc complex were grown in 0.12 M monosaccharides mix, 0.1 M buffer system 3 (pH 8.5), 30 % v/v precipitant mix 1 (Morpheus crystallization screen from Molecular Dimensions). Crystals of the EndoS-Fc complex were grown in 0.09 M halogens, 0.1 M buffer system 2 (pH 7.5), 37.5 % v/v precipitant mix 4 (Morpheus crystallization screen from Molecular Dimensions). Crystals of IgG1 Fc E382S was grown in 0.2 M ammonium sulphate, 0.1 M Tris (pH 7.5), 25 % w/v PEG 8000. Crystals were cryo-protected in mother liquor with 20 % glycerol added and flash-frozen in liquid nitrogen.

Data Collection

Data collection was carried out at the European Radiation Synchrotron Facility (Grenoble, France) for IdeS-Fc and Fc E382S (beamline ID30A-3), and Diamond Light Source (Oxford, UK) for EndoS-Fc (beamline I03).

Structure Determination

Data processing of diffraction images was carried out using DIALS (73) and XDS (74). Structures were solved by molecular replacement with the program Molrep (75). 3AVE was used as a search model to solve the IgG Fc E382S structure; IdeS-Fc and EndoS-Fc were solved using initial search models for the enzyme (PDB code 1Y08 for IdeS; 6EN3 for EndoS), after which the resulting solution was used as a fixed model for a second round of molecular replacement, using 3AVE as the search model. Models were improved with successive rounds of model building and refinement, using Coot (76) and Refmac5 (77), respectively, within the ccp4i2 suite (78). Due to the presence of twinning in the IdeS-Fc data, this structure was refined with the option for twinning ticked in Refmac5. All structures were refined using local non-crystallographic symmetry restraints. PDB-REDO (79) was used to generate restraints for the IgG1 Fc E382S model for use in refinement. MolProbity (51) and the PDB validation server (80, 81) were used for model validation prior to deposition. Carbohydrates were modelled in coot (82) and validated using Privateer (83). Protein complex interfaces were analysed using PISA (47). UCSF ChimeraX (39) was used to prepare figures depicting protein structure.

References

1. M. Collin, A. Olsén, Extracellular enzymes with immunomodulating activities: variations on a theme in Streptococcus pyogenes. *Infect Immun* **71**, 2983-2992 (2003).
2. M. W. Cunningham, Pathogenesis of group A streptococcal infections. *Clin Microbiol Rev* **13**, 470-511 (2000).
3. U. von Pawel-Rammingen, B. P. Johansson, L. Björck, IdeS, a novel streptococcal cysteine proteinase with unique specificity for immunoglobulin G. *EMBO J* **21**, 1607-1615 (2002).
4. M. Collin, A. Olsén, EndoS, a novel secreted protein from Streptococcus pyogenes with endoglycosidase activity on human IgG. *EMBO J* **20**, 3046-3055 (2001).
5. A. Varki *et al.*, Symbol Nomenclature for Graphical Representations of Glycans. *Glycobiology* **25**, 1323-1324 (2015).
6. M. H. Ryan *et al.*, Proteolysis of purified IgGs by human and bacterial enzymes in vitro and the detection of specific proteolytic fragments of endogenous IgG in rheumatoid synovial fluid. *Mol Immunol* **45**, 1837-1846 (2008).
7. R. J. Brezski *et al.*, Tumor-associated and microbial proteases compromise host IgG effector functions by a single cleavage proximal to the hinge. *Proc Natl Acad Sci U S A* **106**, 17864-17869 (2009).
8. T. Lorant *et al.*, Safety, immunogenicity, pharmacokinetics, and efficacy of degradation of anti-HLA antibodies by IdeS (imlifidase) in chronic kidney disease patients. *Am J Transplant* **18**, 2752-2762 (2018).
9. S. C. Jordan, T. Lorant, J. Choi, IgG Endopeptidase in Highly Sensitized Patients Undergoing Transplantation. *N Engl J Med* **377**, 1693-1694 (2017).
10. J. Lin *et al.*, Desensitization using imlifidase and EndoS enables chimerism induction in allosensitized recipient mice. *Am J Transplant* **20**, 2356-2365 (2020).
11. L. Winstedt *et al.*, Complete Removal of Extracellular IgG Antibodies in a Randomized Dose-Escalation Phase I Study with the Bacterial Enzyme IdeS--A Novel Therapeutic Opportunity. *PLoS One* **10**, e0132011 (2015).
12. S. Ge *et al.*, Imlifidase Inhibits HLA Antibody-mediated NK Cell Activation and Antibody-dependent Cell-mediated Cytotoxicity (ADCC) In Vitro. *Transplantation* **104**, 1574-1579 (2020).
13. B. E. Lonze *et al.*, IdeS (Imlifidase): A Novel Agent That Cleaves Human IgG and Permits Successful Kidney Transplantation Across High-strength Donor-specific Antibody. *Ann Surg* **268**, 488-496 (2018).
14. E. Huang, A. Q. Maldonado, C. Kjellman, S. C. Jordan, Imlifidase for the treatment of anti-HLA antibody-mediated processes in kidney transplantation. *Am J Transplant* **22**, 691-697 (2022).
15. S. C. Jordan *et al.*, Imlifidase Desensitization in Crossmatch-positive, Highly Sensitized Kidney Transplant Recipients: Results of an International Phase 2 Trial (Highdes). *Transplantation* **105**, 1808-1817 (2021).
16. C. Kjellman *et al.*, Outcomes at 3 years posttransplant in imlifidase-desensitized kidney transplant patients. *Am J Transplant* **21**, 3907-3918 (2021).
17. M. Crispin, Therapeutic potential of deglycosylated antibodies. *Proc Natl Acad Sci U S A* **110**, 10059-10060 (2013).

18. R. Yang *et al.*, Successful treatment of experimental glomerulonephritis with IdeS and EndoS, IgG-degrading streptococcal enzymes. *Nephrol Dial Transplant* **25**, 2479-2486 (2010).
19. K. S. Nandakumar, B. P. Johansson, L. Björck, R. Holmdahl, Blocking of experimental arthritis by cleavage of IgG antibodies in vivo. *Arthritis Rheum* **56**, 3253-3260 (2007).
20. K. S. Nandakumar *et al.*, Dominant suppression of inflammation by glycan-hydrolyzed IgG. *Proc Natl Acad Sci U S A* **110**, 10252-10257 (2013).
21. C. Lood *et al.*, IgG glycan hydrolysis by endoglycosidase S diminishes the proinflammatory properties of immune complexes from patients with systemic lupus erythematosus: a possible new treatment? *Arthritis Rheum* **64**, 2698-2706 (2012).
22. M. Segelmark, L. Björck, Streptococcal Enzymes as Precision Tools Against Pathogenic IgG Autoantibodies in Small Vessel Vasculitis. *Front Immunol* **10**, 2165 (2019).
23. C. Kizlik-Masson *et al.*, Cleavage of anti-PF4/heparin IgG by a bacterial protease and potential benefit in heparin-induced thrombocytopenia. *Blood* **133**, 2427-2435 (2019).
24. R. Takahashi, N. Yuki, Streptococcal IdeS: therapeutic potential for Guillain-Barré syndrome. *Sci Rep* **5**, 10809 (2015).
25. B. P. Johansson, O. Shannon, L. Björck, IdeS: a bacterial proteolytic enzyme with therapeutic potential. *PLoS One* **3**, e1692 (2008).
26. F. Uhlin *et al.*, Endopeptidase Cleavage of Anti-Glomerular Basement Membrane Antibodies in vivo in Severe Kidney Disease: An Open-Label Phase 2a Study. *J Am Soc Nephrol* **33**, 829-838 (2022).
27. C. Leborgne *et al.*, IgG-cleaving endopeptidase enables in vivo gene therapy in the presence of anti-AAV neutralizing antibodies. *Nat Med* **26**, 1096-1101 (2020).
28. S. Järnum *et al.*, Enzymatic Inactivation of Endogenous IgG by IdeS Enhances Therapeutic Antibody Efficacy. *Mol Cancer Ther* **16**, 1887-1897 (2017).
29. K. Baruah *et al.*, Selective deactivation of serum IgG: a general strategy for the enhancement of monoclonal antibody receptor interactions. *J Mol Biol* **420**, 1-7 (2012).
30. J. J. Goodfellow *et al.*, An endoglycosidase with alternative glycan specificity allows broadened glycoprotein remodelling. *J Am Chem Soc* **134**, 8030-8033 (2012).
31. J. Sjögren *et al.*, EndoS2 is a unique and conserved enzyme of serotype M49 group A Streptococcus that hydrolyses N-linked glycans on IgG and α1-acid glycoprotein. *Biochem J* **455**, 107-118 (2013).
32. E. H. Klontz *et al.*, Molecular Basis of Broad Spectrum N-Glycan Specificity and Processing of Therapeutic IgG Monoclonal Antibodies by Endoglycosidase S2. *ACS Cent Sci* **5**, 524-538 (2019).
33. W. Huang, J. Giddens, S. Q. Fan, C. Toonstra, L. X. Wang, Chemoenzymatic glycoengineering of intact IgG antibodies for gain of functions. *J Am Chem Soc* **134**, 12308-12318 (2012).
34. X. Tong, T. Li, C. Li, L. X. Wang, Generation and Comparative Kinetic Analysis of New Glycosynthase Mutants from Streptococcus pyogenes Endoglycosidases for Antibody Glycoengineering. *Biochemistry* **57**, 5239-5246 (2018).
35. B. Vincents, U. von Pawel-Rammingen, L. Björck, M. Abrahamson, Enzymatic characterization of the streptococcal endopeptidase, IdeS, reveals that it is a

cysteine protease with strict specificity for IgG cleavage due to exosite binding. *Biochemistry* **43**, 15540-15549 (2004).

36. B. Trastoy *et al.*, Crystal structure of Streptococcus pyogenes EndoS, an immunomodulatory endoglycosidase specific for human IgG antibodies. *Proc Natl Acad Sci U S A* **111**, 6714-6719 (2014).
37. E. V. Dixon *et al.*, Fragments of bacterial endoglycosidase s and immunoglobulin g reveal subdomains of each that contribute to deglycosylation. *J Biol Chem* **289**, 13876-13889 (2014).
38. B. Trastoy *et al.*, Structural basis for the recognition of complex-type N-glycans by Endoglycosidase S. *Nat Commun* **9**, 1874 (2018).
39. E. F. Pettersen *et al.*, UCSF ChimeraX: Structure visualization for researchers, educators, and developers. *Protein Sci* **30**, 70-82 (2021).
40. R. Vindebro, C. Spoerry, U. von Pawel-Rammingen, Rapid IgG heavy chain cleavage by the streptococcal IgG endopeptidase IdeS is mediated by IdeS monomers and is not due to enzyme dimerization. *FEBS Lett* **587**, 1818-1822 (2013).
41. B. Lei *et al.*, Opsonophagocytosis-inhibiting mac protein of group a streptococcus: identification and characteristics of two genetic complexes. *Infect Immun* **70**, 6880-6890 (2002).
42. R. Coulombe *et al.*, Structure of human procathepsin L reveals the molecular basis of inhibition by the prosegment. *EMBO J* **15**, 5492-5503 (1996).
43. M. Cygler *et al.*, Structure of rat procathepsin B: model for inhibition of cysteine protease activity by the proregion. *Structure* **4**, 405-416 (1996).
44. J. Sivaraman, M. Lalumière, R. Ménard, M. Cygler, Crystal structure of wild-type human procathepsin K. *Protein Sci* **8**, 283-290 (1999).
45. K. Wenig *et al.*, Structure of the streptococcal endopeptidase IdeS, a cysteine proteinase with strict specificity for IgG. *Proc Natl Acad Sci U S A* **101**, 17371-17376 (2004).
46. J. Agniswamy *et al.*, Crystal structure of group A streptococcus Mac-1: insight into dimer-mediated specificity for recognition of human IgG. *Structure* **14**, 225-235 (2006).
47. E. Krissinel, K. Henrick, Inference of macromolecular assemblies from crystalline state. *J Mol Biol* **372**, 774-797 (2007).
48. R. Bockermann *et al.*, Imlifidase-generated Single-cleaved IgG: Implications for Transplantation. *Transplantation* 10.1097/TP.0000000000004031 (2021).
49. J. J. Söderberg, P. Engström, U. von Pawel-Rammingen, The intrinsic immunoglobulin g endopeptidase activity of streptococcal Mac-2 proteins implies a unique role for the enzymatically impaired Mac-2 protein of M28 serotype strains. *Infect Immun* **76**, 2183-2188 (2008).
50. V. B. Chen *et al.*, MolProbity: all-atom structure validation for macromolecular crystallography. *Acta Crystallogr D Biol Crystallogr* **66**, 12-21 (2010).
51. C. J. Williams *et al.*, MolProbity: More and better reference data for improved all-atom structure validation. *Protein Sci* **27**, 293-315 (2018).
52. G. Oanca, M. Asadi, A. Saha, B. Ramachandran, A. Warshel, Exploring the Catalytic Reaction of Cysteine Proteases. *J Phys Chem B* **124**, 11349-11356 (2020).
53. L. Polgár, P. Halász, Current problems in mechanistic studies of serine and cysteine proteinases. *Biochem J* **207**, 1-10 (1982).

54. D. J. Creighton, M. S. Gessouroun, J. M. Heapes, Is the thiolate--imidazolium ion pair the catalytically important form of papain? *FEBS Lett* **110**, 319-322 (1980).
55. S. D. Lewis, F. A. Johnson, J. A. Shafer, Potentiometric determination of ionizations at the active site of papain. *Biochemistry* **15**, 5009-5017 (1976).
56. X. Zhai, T. D. Meek, Catalytic Mechanism of Cruzain from Trypanosoma cruzi As Determined from Solvent Kinetic Isotope Effects of Steady-State and Pre-Steady-State Kinetics. *Biochemistry* **57**, 3176-3190 (2018).
57. M. A. Villamil, J. Chen, Q. Liang, Z. Zhuang, A noncanonical cysteine protease USP1 is activated through active site modulation by USP1-associated factor 1. *Biochemistry* **51**, 2829-2839 (2012).
58. J. Briliūtė *et al.*, Complex N-glycan breakdown by gut Bacteroides involves an extensive enzymatic apparatus encoded by multiple co-regulated genetic loci. *Nat Microbiol* **4**, 1571-1581 (2019).
59. V. Rao, T. Cui, C. Guan, P. Van Roey, Mutations of endo-beta-N-acetylglucosaminidase H active site residueAs sp130 anG glu132: activities and conformations. *Protein Sci* **8**, 2338-2346 (1999).
60. V. Rao, C. Guan, P. Van Roey, Crystal structure of endo-beta-N-acetylglucosaminidase H at 1.9 A resolution: active-site geometry and substrate recognition. *Structure* **3**, 449-457 (1995).
61. H. Seki *et al.*, Structural basis for the specific cleavage of core-fucosylated N-glycans by endo-β-N-acetylglucosaminidase from the fungus Cordyceps militaris. *J Biol Chem* **294**, 17143-17154 (2019).
62. I. Stals *et al.*, High resolution crystal structure of the endo-N-Acetyl-β-D-glucosaminidase responsible for the deglycosylation of Hypocrea jecorina cellulases. *PLoS One* **7**, e40854 (2012).
63. P. Van Roey, V. Rao, T. H. Plummer, A. L. Tarentino, Crystal structure of endo-beta-N-acetylglucosaminidase F1, an alpha/beta-barrel enzyme adapted for a complex substrate. *Biochemistry* **33**, 13989-13996 (1994).
64. C. A. Waddling, T. H. Plummer, A. L. Tarentino, P. Van Roey, Structural basis for the substrate specificity of endo-beta-N-acetylglucosaminidase F(3). *Biochemistry* **39**, 7878-7885 (2000).
65. M. García-Alija *et al.*, Mechanism of cooperative N-glycan processing by the multi-modular endoglycosidase EndoE. *Nat Commun* **13**, 1137 (2022).
66. M. F. Jennewein, G. Alter, The Immunoregulatory Roles of Antibody Glycosylation. *Trends Immunol* **38**, 358-372 (2017).
67. L. N. Deis *et al.*, Suppression of conformational heterogeneity at a protein-protein interface. *Proc Natl Acad Sci U S A* **112**, 9028-9033 (2015).
68. M. Frank, R. C. Walker, W. N. Lanzilotta, J. H. Prestegard, A. W. Barb, Immunoglobulin G1 Fc domain motions: implications for Fc engineering. *J Mol Biol* **426**, 1799-1811 (2014).
69. A. W. Barb *et al.*, NMR characterization of immunoglobulin G Fc glycan motion on enzymatic sialylation. *Biochemistry* **51**, 4618-4626 (2012).
70. A. W. Barb, J. H. Prestegard, NMR analysis demonstrates immunoglobulin G N-glycans are accessible and dynamic. *Nat Chem Biol* **7**, 147-153 (2011).
71. H. S. Lee, W. Im, Effects of N-Glycan Composition on Structure and Dynamics of IgG1 Fc and Their Implications for Antibody Engineering. *Sci Rep* **7**, 12659 (2017).

72. A. M. Harbison, L. P. Brosnan, K. Fenlon, E. Fadda, Sequence-to-structure dependence of isolated IgG Fc complex biantennary N-glycans: a molecular dynamics study. *Glycobiology* **29**, 94-103 (2019).
73. G. Winter *et al.*, DIALS: implementation and evaluation of a new integration package. *Acta Crystallogr D Struct Biol* **74**, 85-97 (2018).
74. W. Kabsch, XDS. *Acta Crystallogr D Biol Crystallogr* **66**, 125-132 (2010).
75. A. Vagin, A. Teplyakov, Molecular replacement with MOLREP. *Acta Crystallogr D Biol Crystallogr* **66**, 22-25 (2010).
76. P. Emsley, B. Lohkamp, W. G. Scott, K. Cowtan, Features and development of Coot. *Acta Crystallogr D Biol Crystallogr* **66**, 486-501 (2010).
77. G. N. Murshudov *et al.*, REFMAC5 for the refinement of macromolecular crystal structures. *Acta Crystallogr D Biol Crystallogr* **67**, 355-367 (2011).
78. L. Potterton *et al.*, CCP4i2: the new graphical user interface to the CCP4 program suite. *Acta Crystallogr D Struct Biol* **74**, 68-84 (2018).
79. R. P. Joosten, F. Long, G. N. Murshudov, A. Perrakis, The PDB_REDO server for macromolecular structure model optimization. *IUCrJ* **1**, 213-220 (2014).
80. H. Berman, K. Henrick, H. Nakamura, Announcing the worldwide Protein Data Bank. *Nat Struct Biol* **10**, 980 (2003).
81. S. Gore *et al.*, Validation of Structures in the Protein Data Bank. *Structure* **25**, 1916-1927 (2017).
82. P. Emsley, M. Crispin, Structural analysis of glycoproteins: building N-linked glycans with Coot. *Acta Crystallogr D Struct Biol* **74**, 256-263 (2018).
83. J. Agirre *et al.*, Privateer: software for the conformational validation of carbohydrate structures. *Nat Struct Mol Biol* **22**, 833-834 (2015).